Two Propagation Pathways of the Boreal Summer Quasi-Biweekly Oscillation of the Atmospheric Heat Source Over the Tibetan Plateau

Shanshan Zhong, Qiao Jia, Zhiwei Zhu & Xinchang Zhang

Two Propagation Pathways of the Boreal Summer Quasi-Biweekly Oscillation of the Atmospheric Heat Source Over the Tibetan Plateau

Shanshan Zhong*, Qiao Jia, Zhiwei Zhu, and Xinchang Zhang

Key Laboratory of Meteorological Disaster, Ministry of Education (KLME), Joint International Research Laboratory of Climate and Environment Change (ILCEC), Collaborative Innovation Center on Forecast and Evaluation of Meteorological Disasters (CIC-FEMD), Nanjing University of Information Science and Technology, Nanjing 210044, People's Republic of China

ABSTRACT   *Based on the daily Japanese 55-year Reanalysis data, the characteristics of the summer (June–July–August) quasi-biweekly oscillation (QBWO) of atmospheric apparent heat sources over the Tibetan Plateau (TP) and its surrounding areas (TPSR) are investigated. The first three leading modes of the atmospheric intraseasonal heat source over the TPSR reflect two independent propagation features of the QBWO. The first, which propagates from east to west, is associated with the mid- to upper tropospheric circulation, with large-scale anomalous cyclones and anticyclones propagating from northeast China, across the TP, and finally arriving in West Asia. The intensity of this QBWO rapidly increases when approaching the TP and significantly weakens during its westward journey upon leaving the TP. The second, which moves from west to east, is closely correlated with the mid-latitude Rossby wave train emanating from southern Europe that travels over the TP to the East Asian coast. Remarkable differences can be observed between the intensity of the wave train over the east and west sides of the TP. To the west of 90°E, the QBWO strengthens when proceeding to the TP and reaches its maximum over the TP. To the east of 90°E, the circulation anomalies are maintained for about half a cycle. For both propagation pathways, the QBWO of the heat source over the TPSR greatly modulates the circulation and precipitation anomalies over the TP, the Indian Peninsula, and the Indochina Peninsula.*

RÉSUMÉ   *[Traduit par la rédaction] Nous étudions les caractéristiques estivales (juin, juillet et août) de l'oscillation quasi bimensuelle de la source de chaleur atmosphérique apparente sur le plateau tibétain et ses environs, et ce, à partir de 55 années de données quotidiennes de réanalyse venant du Japon. Les trois premiers modes de la source de chaleur atmosphérique intrasaisonnière sur la région du plateau tibétain reflètent pour cette oscillation deux types de propagation indépendants. Le premier mode, qui se propage d'est en ouest, est associé à la circulation de la troposphère moyenne à supérieure, et présente des cyclones et des anticyclones anormaux de grande échelle, qui se déplacent du nord-est de la Chine vers le plateau tibétain pour finalement arriver en Asie occidentale. L'intensité de cette oscillation quasi bimensuelle augmente à l'approche du plateau tibétain et s'affaiblit considérablement au cours de son trajet vers l'ouest, passé ce plateau. Le second mode, qui se déplace d'ouest en est, est étroitement corrélé au train d'ondes de Rossby des latitudes moyennes, qui provient du sud de l'Europe et se déplace du plateau tibétain jusqu'à la côte de l'Asie orientale. Nous observons des différences remarquables dans l'intensité du train d'ondes sur les parties est et ouest du plateau tibétain. À l'ouest de 90° E, l'oscillation quasi bimensuelle se renforce en se dirigeant vers le plateau et atteint son maximum au-dessus de celui-ci. À l'est de 90° E, les anomalies de la circulation persistent sur environ un demi-cycle. Pour ces deux types de propagation, l'oscillation de la source de chaleur sur la région du plateau tibétain module fortement les anomalies de circulation et de précipitations sur ce plateau, la péninsule indienne et l'Asie du Sud-Est*

KEYWORDS   Tibetan Plateau; diabatic heating; quasi-biweekly oscillation (QBWO); propagation pathways

1 Introduction

The existence of heat sources in the atmosphere is the most fundamental cause of the continual changes in atmospheric movement. Since Ye, Luo, and Zhu (1957) and Flohn (1957) discovered that the Tibetan Plateau (TP) is a source of heat to the atmosphere in boreal summer, in-depth studies have been devoted to unravelling the thermal impact of the TP on weather and climate both locally and globally (Li, Lu, Huang, Fan, & Zhang, 2016; Lin & Wu, 2011, 2012; Wu et al., 2006; Wu, Jiang, Li, Zhong, & Wang, 2012; Wu, Li,

*Corresponding author's email: zhongshanshan@nuist.edu.cn

Jiang, & Ma, 2012; Wu, Zhang, Chen, & Li, 2016; Yanai, Li, & Song, 1992). Ye and Wu (1998) proposed the concept of an air pump over the TP driven by sensible heat: the strong descending motion over the surrounding regions of the TP (TPSR) during winter and the strong ascending motion in summer act as a huge air pump that regulates atmospheric movements over Asia and worldwide. Chen and Li (1982) suggested that the most intense heat source centre in summer in Asia is located in the northern part of the Bay of Bengal (BOB) and the South China Sea–West Pacific Ocean. Although the strongest centre of the entire layer of atmospheric heat is not over the TP, its intensity over the TP and the BOB is comparable in terms of the maximum heating rate per unit thickness (Zhong, He, Guan, & Wen, 2009; Zhong, Wu, & He, 2013). Thus, it can be seen that the TP constitutes a huge "heat source column" embedded in the middle of the troposphere, and its thermal forcing could modulate the precipitation and water vapour transport in eastern China (Xu, Zhao, Shi, & Lu, 2015), which are essential to the formation of and changes in the Asian monsoon (Duan & Wu, 2005; Wu & Zhang, 1998; Wu, Liu, et al., 2012).

The Intraseasonal Oscillation (ISO) with a time scale between 10 and 90 days is one of the most significant climatic phenomena and is ubiquitous in both the troposphere and stratosphere over the tropics and extratropics. Numerous observational studies have confirmed that the TPSR is one of the most active regions of the ISO in the mid-latitudes (Wang & Duan, 2015; Wang, Dai, Guo, & Ge, 2017; Wang, Wang, Duan, Liu, & Zhou, 2018). Wang and Duan (2015) used 30 years of data to analyze the meteorological factors and found that there are three periods of atmospheric low-frequency oscillations over the TP: 10–20 days (the quasi-biweekly oscillation; QBWO), 7–9 days, and over 30 days. Many studies have shown that the periodicities of the ISO over the TP mostly depend on meteorological elements and samples (Fujinami & Yasunari, 2004; Hu, Duan, Li, & He, 2016; Yang et al., 2017).

The propagation features and the origins of the ISO over the TPSR are very complicated. Liu, Hoskins, and Blackburn (2007) found that strong diabatic heating over the TP in summer excites a zonal asymmetric instability, leading to the appearance of the QBWO of the South Asia High in the region. Wang and Duan (2015) pointed out that the QBWO of the diabatic heating over the TP originates from the western equatorial Pacific, which travels clockwise through the BOB and northern India, north to the southeast of the plateau, and finally eastward to East Asia. In addition, the ISO over the TP is also related to the disturbance of the mid-latitude wave. The conversion between the dry and the wet phases of the ISO over the eastern TP is related to the Rossby wave train, which is characterized by large anomalous anticyclonic and cyclonic centres alternating along the path from the eastern Atlantic Ocean over the TP to southern China (Hu et al., 2016). Yang et al. (2017) confirmed that the ISO activity over the TP is closely related to the mid-latitude and tropical non-stationary wave trains moving along

different pathways. Yang and Li (2017) revealed two main modes of the ISO of the diabatic heating over the TP in summer and their causes. The first main mode is the quasi-stationary type centred on the southern plateau, which has a variability of 10–30 days that is mainly caused by the west-ward propagation of the ISO disturbance in the tropical western Pacific. The second is the east–west asymmetric dipole type, the formation of which relates to the important role played by the mid-latitude Rossby wave propagating southeastward toward the plateau. The ISO anomaly signal propagates clockwise, from the northwest to the eastern part of the TP. Meanwhile, the opposite anomalous signal propagates from the southeast to the western part of the TP. Furthermore, the unique terrain and the thermal effect of the TP can promote the formation of the ISO, and these factors will maintain intraseasonal Rossby waves.

The ISO over the TP can strongly influence the occurrence and development of floods in the northern hemisphere (Duan, Wu, Liu, Ma, & Zhao, 2012; Tao & Ding, 1981; Zhang, Li, Fu, Liu, & Li, 2014) by changing the corresponding down-stream circulation field (Fujinami & Yasunari, 2004, 2009; Liu, Yang, Zhang, & Wang, 2014; Watanabe & Yamazaki, 2012; Yang et al., 2014, 2017; Yasunari & Miwa, 2006). The ISO over the TP has a definite influence on the weather systems, such as the plateau vortex, the subtropical high, and the south Asian high, thus causing weather and climate anomalies. For example, the ISO over the TP can trigger severe summer flood and drought conditions in the lower reaches of the Yangtze River in China (Yang & Li, 2003).

In summary, the intraseasonal variability of diabatic heating over the TP may be a potential predictor that can be used to improve extended-range forecasts of local and East Asian weather and climate. However, the propagation features of the ISO of the atmospheric heat source over the TP remains unclear.

The present study aims to unravel the propagation pathways of the boreal summer QBWO of the atmospheric heat source over the TPSR. The rest of the paper is structured as follows. Section 2 describes the data and methods. The climatology of the summer atmospheric heat source over the TP is presented in Section 3. The leading modes of the summer QBWO of the intraseasonal heat source over the TP are described in Section 4. The QBWO propagation of the summer heat source over the TPSR is discussed in Section 5. Finally, a summary is given in Section 6.

2 Data and methods

The datasets employed in this study include (i) the daily Japanese 55-year Reanalysis (JRA-55) from 1979 to 2018 with a horizontal resolution of $1.25° \times 1.25°$, which includes the wind field, temperature, and potential height of 37 vertical levels ranging from 1000 to 1 hPa (Kobayashi et al., 2015); (ii) the daily outgoing longwave radiation (OLR) data from the National Oceanic and Atmospheric Administration from 1979 to 2018 with a horizontal resolution of $2.5° \times 2.5°$ (Liebmann & Smith, 1996); and (iii) the daily global
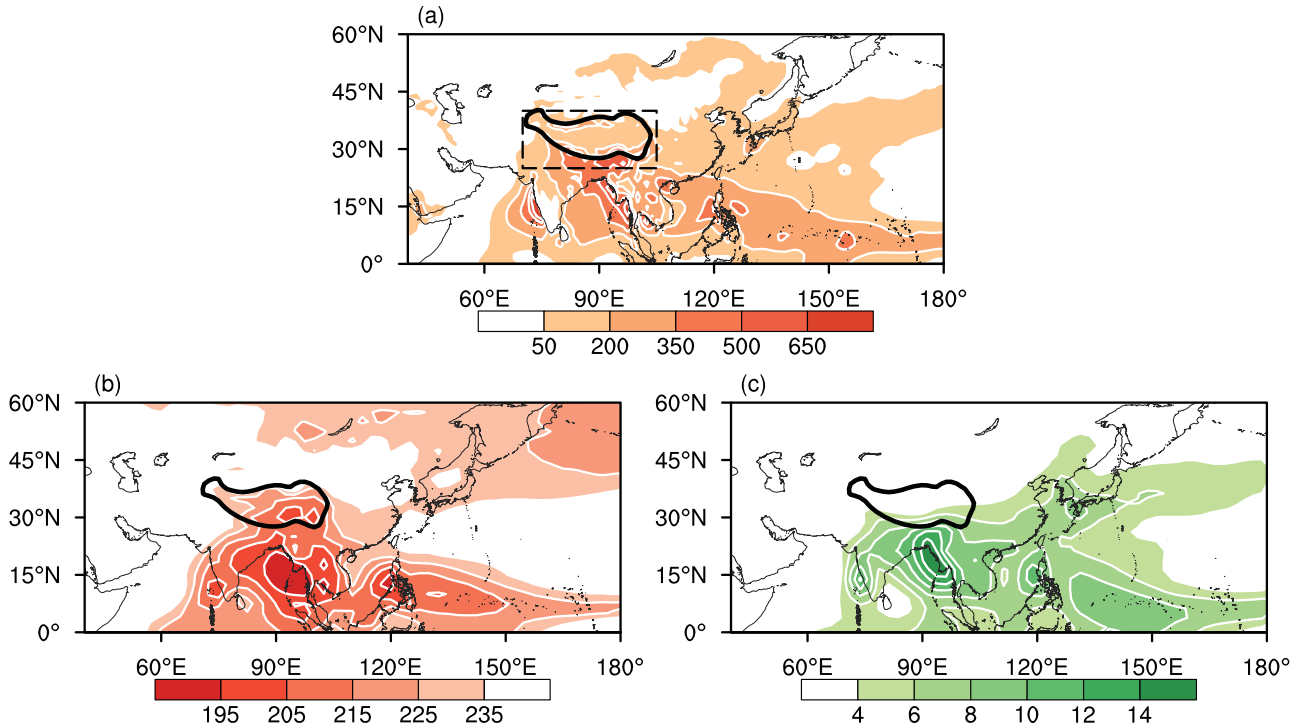
Fig. 1   Horizontal distribution of the (a) whole-layer atmospheric heat source (W m^{-2}), (b) OLR (W m^{-2}), and (c) precipitation (mm) in the summers from 1979 to 2018 (the black solid line indicates the 3000 m terrain contour; the dotted black rectangle in (a) shows the region of the TPSR).

precipitation from the Global Precipitation Climatology Project (GPCP) during the period 1997–2018 with a horizontal resolution of 1° × 1°.

The atmospheric heat source (Q_1) is calculated using an inverse algorithm (Yanai et al., 1992; Zhong, Wu, & He, 2013). The formula is

$$Q_1 = C_p \left[\frac{\partial T}{\partial t} + \mathbf{V} \cdot \nabla T + \left(\frac{p}{p_0} \right)^k \omega \frac{\partial \theta}{\partial p} \right], \qquad (1)$$

where T is the temperature, ω is the vertical velocity of the pressure coordinate, $p_0 = 1000$ hPa, θ is the potential temperature, and $\mathbf{V}$ is the horizontal wind vector. Assuming a tropopause top of $\omega = 0$, Eq. (1) is integrated over the whole layer of the atmosphere to obtain

$$\langle Q_1 \rangle = \frac{1}{g} \int_{P_t}^{P_s} Q_1 \, dp, \qquad (2)$$

where P_s is the surface pressure and P_t refers to the pressure at the top of the atmosphere ($P_t = 100$ hPa).

The daily atmospheric heat source from 1 June to 31 August (92 days) from 1979 to 2018 is extracted to form a sequence of 40 summers (1979–2018). The seasonal cycle is removed from all data prior to power spectrum analysis and the weather-scale signal is removed using a 5-day moving average. The Lanczos filter method is used to extract the main intraseasonal signals, and corresponding empirical

orthogonal function (EOF) and composite analyses are performed (Duchon, 1979). Statistical methods, such as correlation analysis, North's rule (North, Bell, Cahalan, & Moeng, 1982), and a Student's t-test (Bretherton, Widmann, Dymnikov, Wallace, & Blade, 1999) are also used.

3 Climatology of the summer atmospheric heat source over the TP

The horizontal distribution of the whole-layer atmospheric heat source, $<Q_1>$, in the summers of 1979–2018 (see Fig. 1a) shows that there are two significant heat source zones over Asia. One is centred around the eastern BOB and the southern TP. This large heat source zone stretches from the northwestern coast of the Indochina Peninsula, through the TP, to the western Indian Peninsula and over the eastern Arabian Sea. Three maximum centres appear over the northeastern BOB to the western coast of the Indochina Peninsula, the region to the south of the southern slopes of the TP, and the western coast of the Indian Peninsula, respectively. The other large heat source zone is situated over the South China Sea to the tropical western Pacific, with the strongest centre being near the Philippines. Note that the pattern of this heat source zone resembles the western Pacific monsoon rain belt (Ma, Zhu, Li, & Cao, 2019).

In summer, latent heat from precipitation is the important contributor to atmospheric diabatic heating. The OLR and GPCP precipitation fields are plotted in Figs 1b and 1c. It can be seen that the two heat source zones are basically
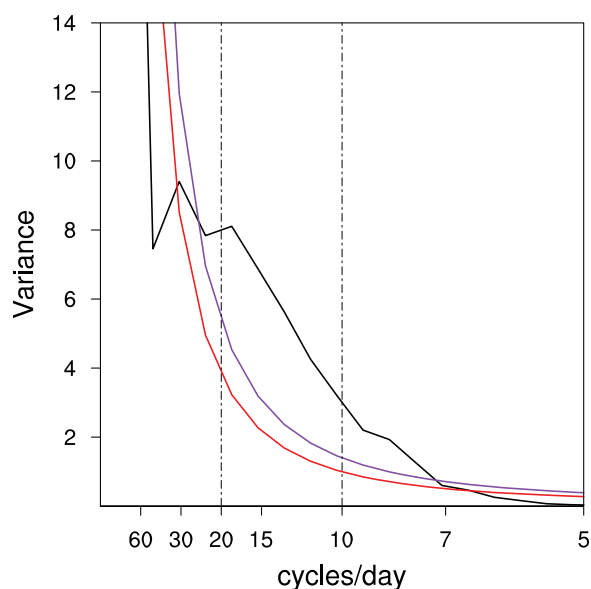
Fig. 2   Power spectrum analysis of the average of the daily atmospheric heat source over the TP and surrounding areas in the summers of 1979–2018 (W m^{-2}) (the red and purple lines represent red noise and the significance level of 0.05, respectively).

To determine the period of the ISO of the atmospheric heat source over the TPSR refer to Yang et al. (2017); the average of the daily heat source over the domain (25°–40°N, 70°–105°E, the black dotted rectangular area in Fig. 1a) is selected to analyze the power spectrum of the heat source. Figure 2 clearly shows that the life cycle of the TPSR heat source is concentrated at a period of 10–20 days, which is the actual band of the QBWO (Hu et al., 2016; Wang & Duan, 2015; Yang et al., 2017). Therefore, in this study, we focus on investigating the QBWO of the diabatic heating source over the TPSR. All variables are first subjected to 10–20 days of band-pass filtering using a Lanczos filter (Duchon, 1979) to extract the quasi-biweekly component of the ISO.

4 Leading modes of the summer QBWO of the intraseasonal heat source over the TP

Figure 3 shows the spatial pattern of the first three modes of the 10–20-day filtered $< Q_1 >$ over the TPSR based on EOF analysis. The first three EOFs explain 16.02%, 11.68%, and 6.36% of the total variance, respectively. These three modes are significantly different from the other modes according to North's criterion (North et al., 1982).

The first mode shows uniformity over the entire TP with a negative loading centre located in the northeastern TP. The second mode presents a southeast–northwest dipole pattern. The northwestern TP is out of phase with the southeastern edge of the TP with respect to the 3000 m isoheight. The third mode shows a zonally asymmetric distribution with

consistent with regions of enhanced convection and the precipitation zone. Therefore, the calculation of the atmospheric heat source based on the JRA-55 dataset in the present study is reasonable and reliable.
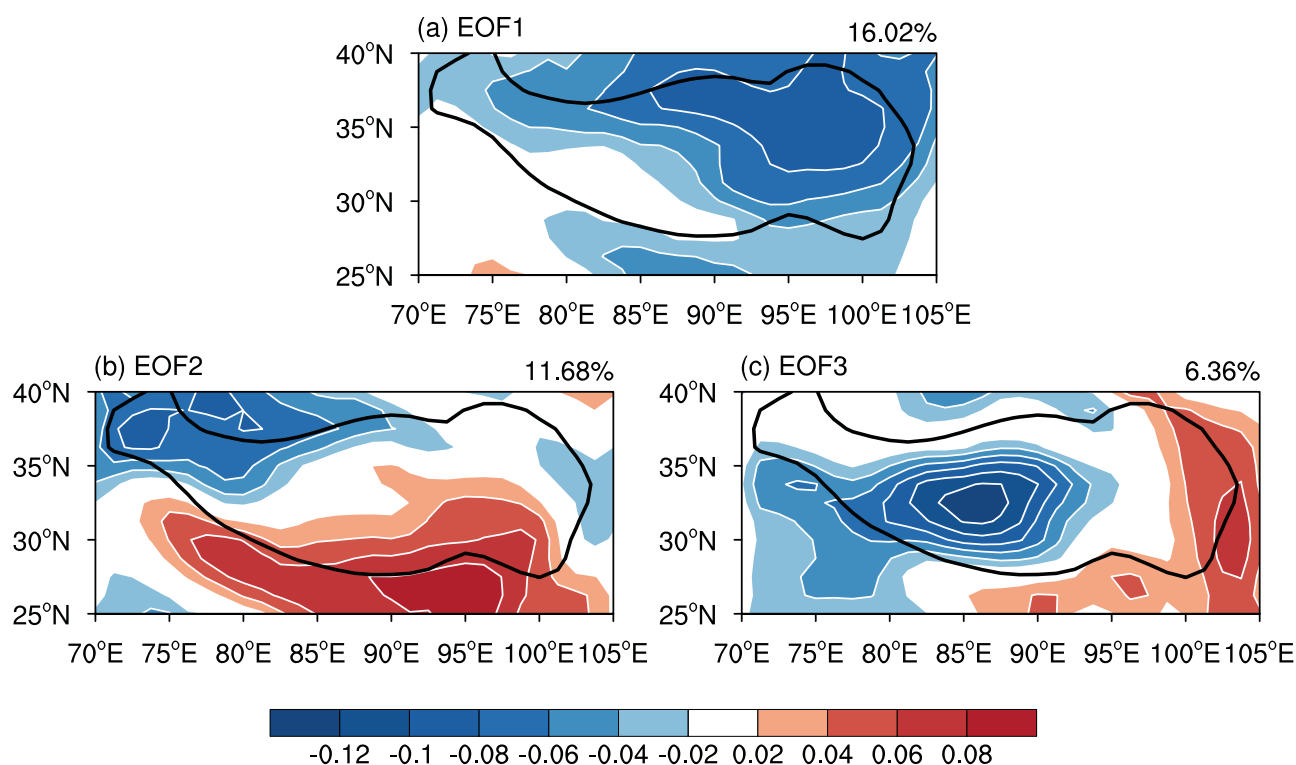

Fig. 3   EOF analysis of the 10–20-day atmospheric heat source over the TPSR in the summers from 1979 to 2018 (the solid black line indicates the 3000 m terrain contour, and the percentage marked in the upper-right corner is the variance contribution of the mode).
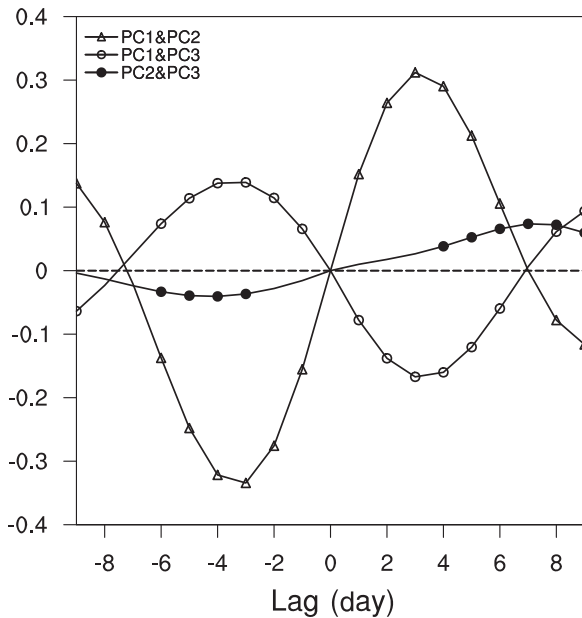
Fig. 4   Lead–lag correlation analysis of the first three modes' time series of the 10–20-day atmospheric heat source over the TPSR in the summers of 1979 to 2018 (only points that pass the significance level of 0.05 are shown). Note: Taking PC1 and PC2 as examples, the positive values of the horizontal axis indicate that PC1 leads PC2, and the negative values indicate that PC1 lags PC2.

negative loading over the western hinterland and positive loading over the eastern border. Notably, because the three leading modes are not statistically independent of each other, the combination of each pair of two modes may reflect the different propagation modes of the QBWO. The negative loading centres of EOF1 and EOF2 are in the northeast and northwest of the TP, respectively, while the negative loading centres of EOF1 and EOF3 are over the northeast and west of the TP, respectively. However, do these two pairs of modes reflect the different propagation modes of the QBWO of the heat source over the TPSR? To address this question, we perform lead–lag correlation analysis among the principal components (PCs) of the three EOF modes.

As shown in Fig. 4, when PC1 leads (lags) PC2 for three days (about one-quarter of the life cycle of the QBWO), the correlation coefficient between the two PCs reaches a maximum (minimum) of 0.31 (−0.33), whereas, when PC1 lags (leads) PC3 for three days, the two PCs have a maximum positive (negative) correlation of 0.14 (−0.17). On the contrary, the lead–lag correlation between PC2 and PC3 is weak although some points of the correlation coefficients in Fig. 4 passed the significance test, they are much smaller than those between PC1 and PC2 (or PC1 and PC3), so they are not analyzed in this study. Therefore, EOF1 and EOF2 can be considered as one QBWO propagation mode of the heat source over the TPSR, while EOF1 and EOF3 together reflect another mode. In the following, phase composite analysis is used to further verify these two propagation modes of the QBWO of the heat source over the TPSR.

Referring to the method of Matthews (2000), the QBWO is represented by a two-dimensional space vector $\mathbf{Z}(t)$:

$$\mathbf{Z}(t) = [\text{PC1}(t),\ \text{PC2}(t)], \tag{3}$$

$$A(t) = [\text{PC1}^2(t) + \text{PC2}^2(t)]^{1/2}, \tag{4}$$

$$\alpha(t) = \tan^{-1}\left[\frac{\text{PC2}(t)}{\text{PC1}(t)}\right], \tag{5}$$

where $A(t)$ is the amplitude and $\alpha(t)$ is the phase angle of PC1 and PC2. According to PC1 and PC2, each QBWO cycle is divided into eight phases, and the interval of the phase angle is $\pi/4$. Figure 5 shows the relationship between the PC and phase angle (α) of the first three modes. When the amplitude of PC1 reaches its maximum value, the phase angle is 0, and the amplitude of PC2 is 0. Three days later (i.e., a phase angle of $\pi/2$), PC2 reaches its maximum value (Fig. 5a). Similarly, when PC3 leads PC1 to reach a maximum value in three days, the phase angle is $-\pi/2$ (Fig. 5b).

To reveal the evolutionary characteristics of the QBWO of the heat source over the TPSR, the life cycle of the QBWO of the heat source is divided into eight phases, and composite analysis is employed on each phase. The composite analysis can be carried out as follows. When PC1 reaches its maximum peak value, the phase angle is 0. According to the size of $\alpha(t)$, each period is divided into 1–8 phases, with the phase angle ranging from $-\pi$ to π. Based on the amplitudes and signs (Fig. 5) of PC1 and PC2 (PC1 and PC3), as shown in Fig. 6, the QBWO of the heat source is projected into 1–8 phases, respectively.

In general, the intensity of the ISO is defined by the sum of the squares of the time coefficients of the two modes (i.e., $\text{PC1}^2 + \text{PC2}^2$) or its square $[(\text{PC1}^2 + \text{PC2}^2)^{1/2}]$. In the present study, we focus on the more intensive QBWO events; therefore, $\text{PC1}^2 + \text{PC2}^2 \geq 1$ and $\text{PC1}^2 + \text{PC3}^2 \geq 1$ are the selection criteria. As shown in Fig. 6, the strong QBWO events are outside the red circle, while the weak ones are inside the circle. Among the eight phases, strong QBWO events account for more than 50% of each phase. In the following, phase composite analysis of the associated meteorological fields is conducted based on phase division, as shown in Fig. 6. Regarding the significance test of the composite analysis, the effective degree of freedom was calculated for the filtered data by a statistical significance test (Student's t-test), which is described in detail in the work of Bretherton et al. (1999).

5 QBWO propagation of the summer heat source over the TPSR

a *Westward Propagation Mode of the QBWO of the Heat Source Over the TP*

The QBWO propagation of the diabatic heating source and OLR fields corresponding to the eight phases composited by PC1 and PC2 are shown in Fig. 7. In Phase 1, between 35°N and 45°N, QBWO heat sources dominate from the North
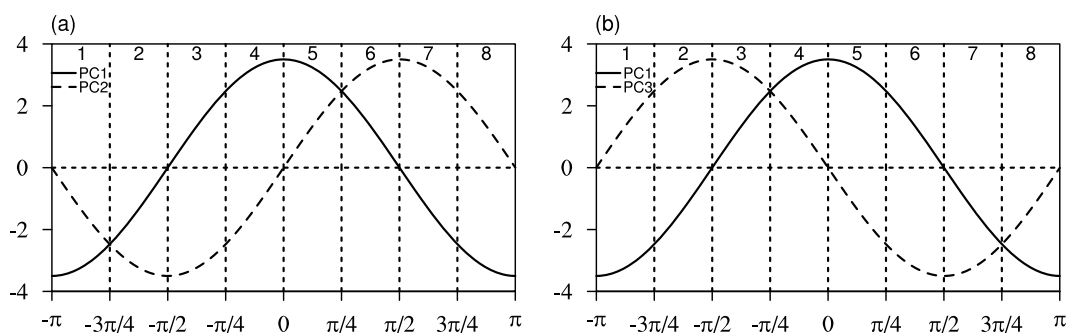
Fig. 5   Schematic diagram of the temporal variation of (a) PC1 and PC2 and (b) PC1 and PC3, corresponding to the phases of the 12-day period (the numbers 1–8 at the top represent the phases).
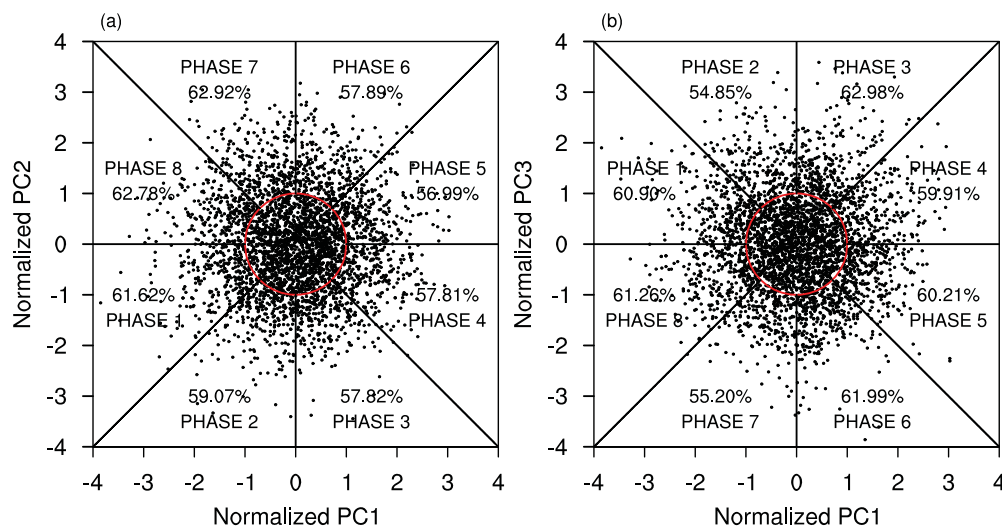

Fig. 6   Distribution of PCs in each phase: (a) PC1 and PC2 and (b) PC1 and PC3. The dots outside the red line show (a) $PC1^2 + PC2^2 > 1$ and (b) $PC1^2 + PC3^2 > 1$; that is, QBWO active events, and the percentage is the ratio of QBWO active events occurring in each phase.

China Plain to the northwest of the TP. In Phase 2, the heat source anomaly moves northwestward to extend from the northwestern TP to the Aral Sea. Meanwhile, a weak negative heat source appears northeast of the TP (i.e., near the Inner Mongolia Plateau). In Phase 3, the positive heat source continues to move westward, while the negative heat source northeast of the TP moves closer to the TP, and the intensity increases rapidly. In Phase 4, the heat source moves westward, out of the TP, with the intensity obviously weakened, and the range contracted to the south. The negative heat source continues to move westward to the TP, controlling the eastern part of the TP, and the intensity enhances rapidly.

During the evolution of the QBWO of the heat source over the TPSR, on the south side of the 3000 m topographic contour of the TP, the heat source of the QBWO changes almost in situ to the form of standing waves. It appears in Phase 2, strengthens in Phase 3, and weakens and gradually disappears in Phases 4 and 5. The sign then changes in Phase 6 and evolves from Phase 6 to Phase 8 with the opposite signs.

In addition, the South China Sea, the western coast of the Indian Peninsula, and the BOB are also active areas of intraseasonal heat sources. The anomalous centres of the former two have no obvious propagation characteristics, while the latter shows propagation to the northwest. In Phases 1–4 (Figs 7a–7d), the heat source spreads northwestward from the eastern coast of the BOB, through the northern part of the Indian peninsula, and reaches the eastern part of the Iranian Plateau. It weakens and disappears after moving out of the plateau's longitudinal range. The negative heat source reappears over the eastern coast of the BOB and the above process is repeated (phases 5–8, Figs 7e–7h).

Throughout their entire life cycles, the centre of the QBWO of OLR corresponds well with the heating centre at low latitudes, while they do not correspond perfectly at mid-latitudes. This is mainly because latent heating in the tropics is the main contributor to the atmospheric heat source, whereas the situation is more complicated in mid-latitudes: latent heating in mid-latitudes is only part of the diabatic heating; sensible heating is also a contributor.

From the above, the first two leading modes of the QBWO of the diabatic heating source over the TPSR is characterized by its propagation from east to west. It comes from the North
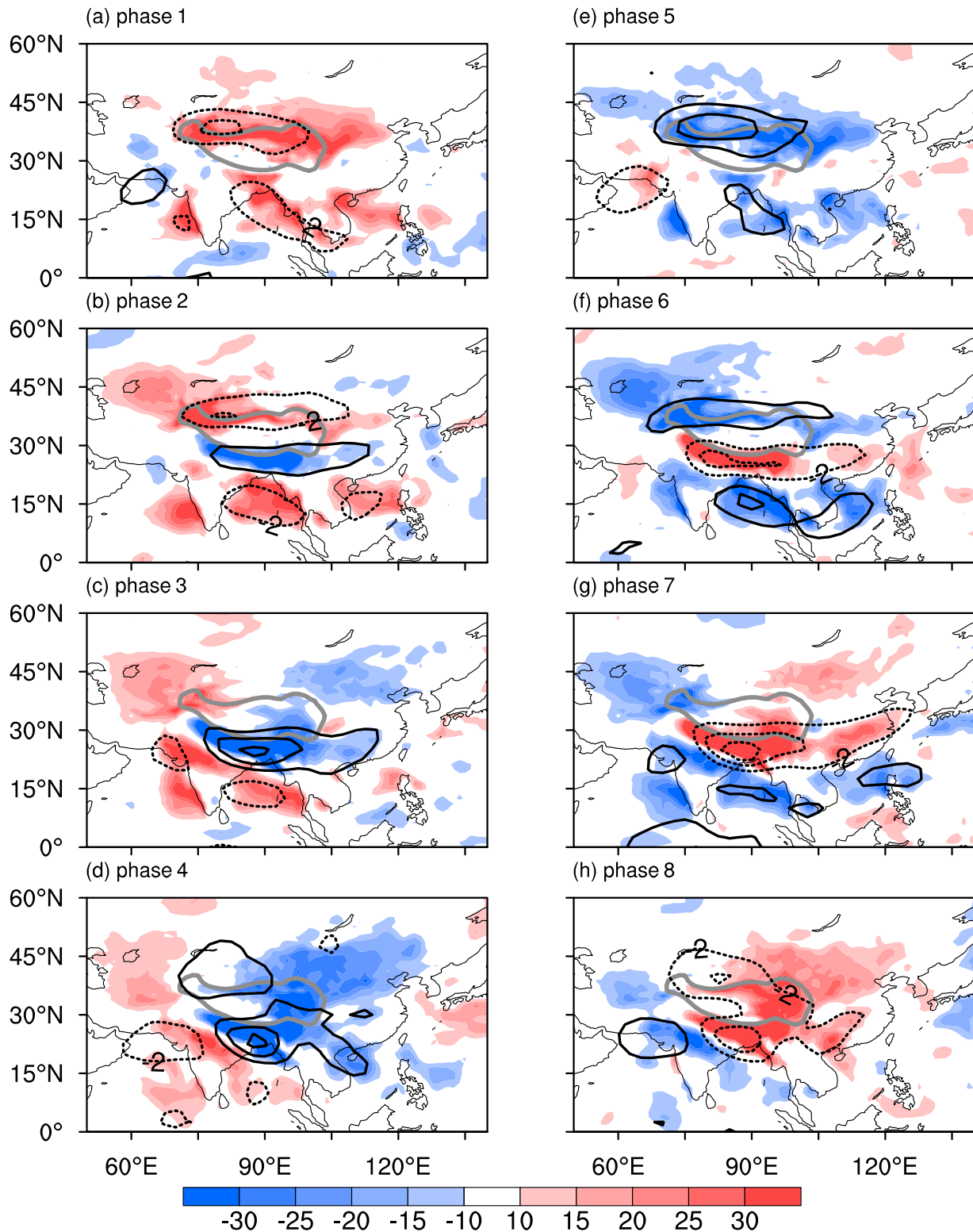
Fig. 7 Evolution of the 10–20-day atmospheric heat source for the summers of 1979–2018 (based on the composite phases of PC1 and PC2) (shading; W m^{-2}) and OLR field (contours; W m^{-2}) (contours and shaded areas are significant at the 0.05 level; solid grey lines indicate the 3000 m terrain contour). The solid and dashed lines represent the positive and negative values, respectively.

China Plain, passes through the TP, and reaches West Asia. The intensity and range are obviously enhanced when moving closer to the TP, and it gradually weakens and disappears when leaving the plateau. At the southern margin of the TP, the QBWO of the heat source manifests mainly in the form of stationary waves.
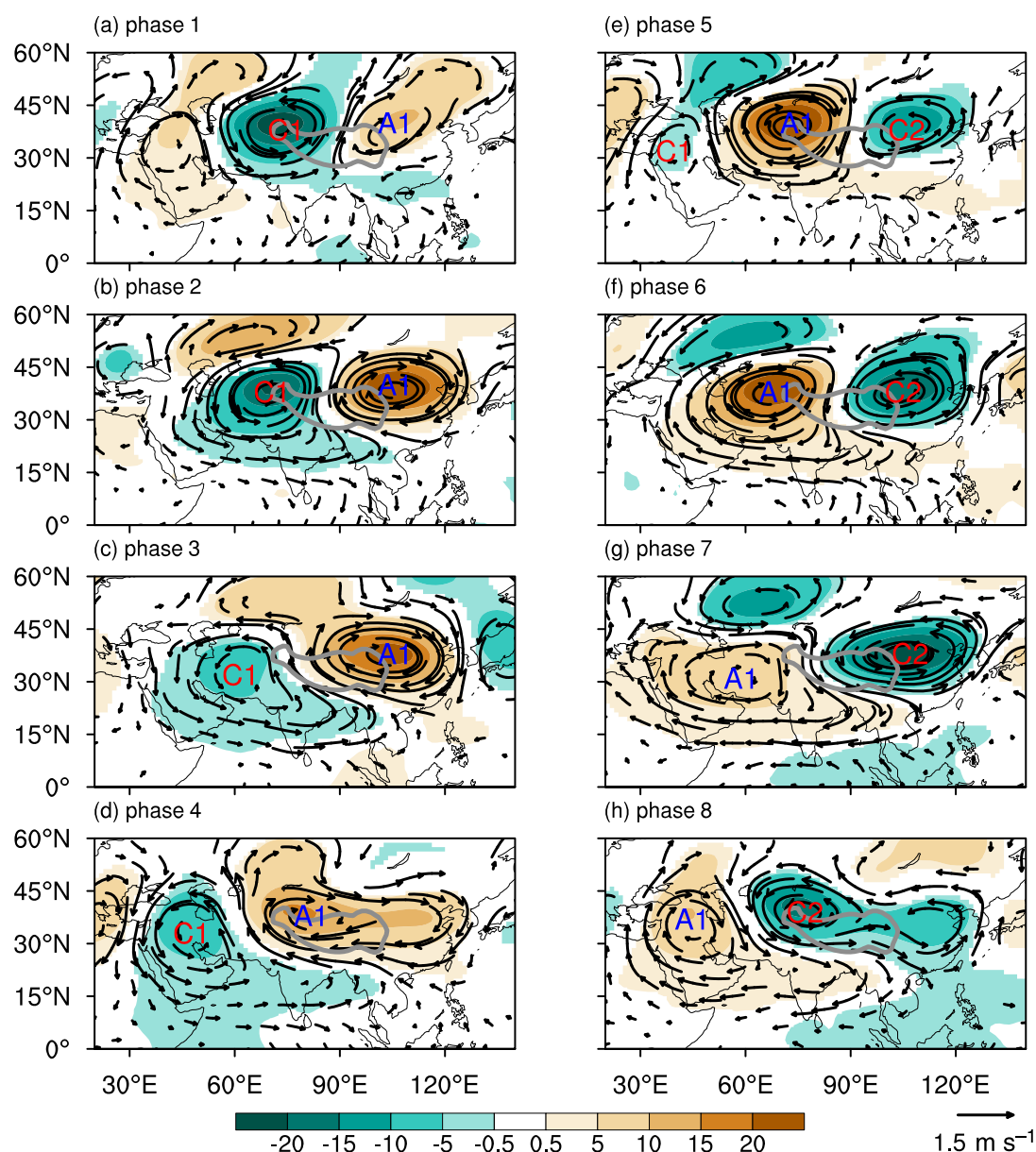
Fig. 8   Evolution of the 200 hPa 10–20-day wind field (vectors; m s^{-1}) and potential height field (shading; gpm) with phase in the summers of 1979–2018 (based on the composite phases of PC1 and PC2) (vectors and shaded areas are significant at the 0.05 level; solid grey lines indicate the 3000 m terrain contour).

Corresponding to the above-mentioned propagation, the evolutionary characteristics of the QBWO at 200 hPa are shown in Fig. 8. The centre of the anomalous circulation is mainly concentrated between 30°N and 45°N. In Phase 1 (Fig. 8a), the western TP is dominated by a large anomalous cyclonic circulation (C1), with a centre over the northwestern part of the TP. Anomalous anticyclonic circulation (A1) over the northeast of the TP follows closely, with a weaker centre from the North China Plain to the Inner Mongolia Plateau in East Asia. As A1 expands toward the TP, C1 is deformed by A1, creating a long and narrow cyclonic shear zone to the southeast (Phase 2, Fig. 8b). In Phase 3 (Fig. 8c), C1 reaches the Iranian Plateau and becomes weaker, while the movement and intensity of the shear

line vary with C1; A1 gradually gains control over the entire plateau, but its centre is still located over the northeast corner of the TP. In Phase 4 (Fig. 8d), C1 arrives at the Arabian Peninsula, and its southeastern shear line also shrinks to the northwest. The A1 circulation centre moves rapidly from the northeast to the northwest of the TP, with a zone of east–west anomalous high pressure establishing over the TP.

In Phases 5–8 (Figs 8e–8h), C1 weakens and disappears; A1 initially strengthens as it moves westward, with its centre eventually located over the northwest of the TP. A new cyclonic anomaly (C2) forms over the northeast of the TP. With the westward movement of A1, C2 gradually gains control of the TP.
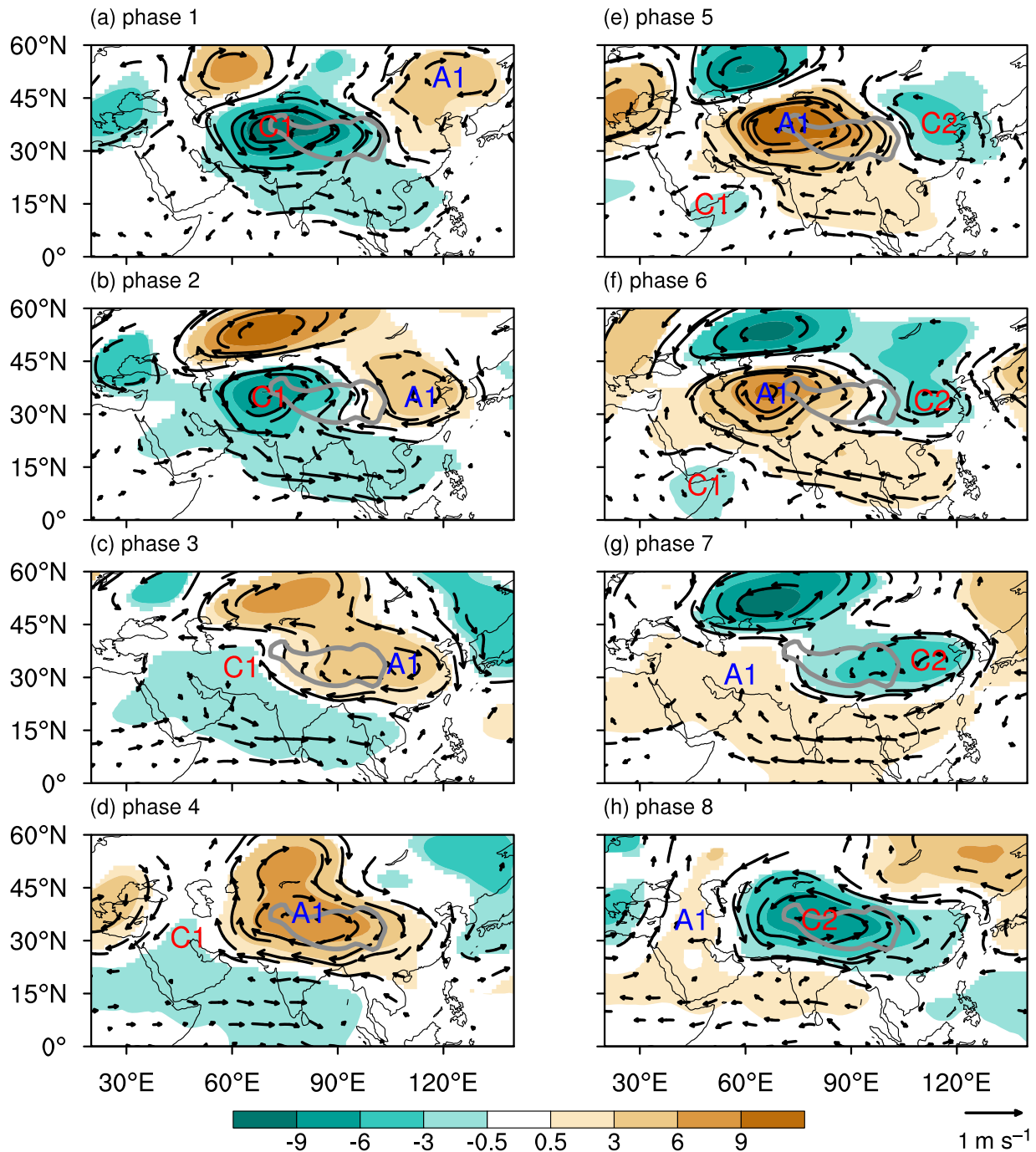
Fig. 9 Evolution of the 500 hPa 10–20-day wind field (vectors; m s^{-1}) and potential height field (shading; gpm) with phase in the summers of 1979–2018 (based on the composite phases of PC1 and PC2) (vectors and shaded areas are significant at the 0.05 level; solid grey lines indicate the 3000 m terrain contour).

The phase evolutions of the geopotential height anomalies and wind circulation anomalies at 500 hPa (Fig. 9) are similar to those at 200 hPa, showing an equivalent barotropic vertical structure. For example, the anomalous circulation centres of C1, A1, and C2 at 500 and 200 hPa are basically consistent. Because of the high altitude of the TP, 500 hPa is equivalent to the near-surface atmosphere of the TP. Thus, compared with 200 hPa, the abnormal circulation over the TP presents a stronger intensity and larger range.

Given the consistent nature of the thermal and thermodynamic fields of the QBWO, in the following, the 500 hPa anomalous circulation field (Fig. 9), the atmospheric diabatic heating field (Fig. 7), and the precipitation field (Fig. 10) are discussed together.

In Phase 1 (as shown in Figs 9a, 7a, and 10a), the anomalous cyclonic circulation, with its centre marked as C1, enhances the thermal low over the surface of the TP, resulting in the heat pump effect of the TP. In the eastern part of C1, the

maximum cyclonic shear is formed by the anomalous south-easterly and southwesterly winds, corresponding to enhancement of the heat source (Fig. 7a). Meanwhile, over the TPSR hinterland and to its east, the horizontal convergence increases the ascent of water vapour, resulting in enhanced precipitation (Fig. 10a).

On the southern flank of C1, the northern part of the BOB to the western coast of the Indochina Peninsula along with the western coast of the Indian Peninsula are under the control of westerly anomalies, resulting in a strengthened southwest monsoon, increased heat and water vapour transport, and formation of an abnormal atmospheric heat source (Fig. 7a) and more precipitation (Fig. 10a). The area south of the Yangtze River is situated within the anomalous eastward airflow at the bottom of the anomalous anticyclonic circulation, A1, with a weakened southwest monsoon, reduced water vapour transport, and less precipitation.

In Phase 2 (Figs 9b, 7b, and 10b), the centre of C1 moves westward to the west of the TP, and its intensity gradually weakens. Meanwhile, the related atmospheric heat source anomalies and precipitation anomalies move westward. The anomalous anticyclonic circulation, A1, approaches the east side of the TP and strengthens. Deformed by the extrusion of A1, C1 elongates resulting in a long and narrow cyclonic shear zone to the southeast, which is consistent with the evolution of the circulation at 200 hPa. Because the Indian Peninsula, the BOB, and the South China Sea are located to the south of the shear line, where the westerly anomaly prevails and the southwest monsoon, moisture convergence, and diabatic heating are enhanced, a northwest–southeast elongated zone of positive precipitation anomalies is formed. By contrast, a zone of less precipitation appears on the southern side of the TP (Fig. 10b). This is because the southern edge of the TP lies on the north side of the shear line, where an easterly anomaly prevails, and the monsoon is weakened. The weakened monsoon further acts to hinder the convergence of water vapour leading to a negative heat source anomaly (Fig. 7b).

In Phases 3–4 (Figs 9c and 9d, 7c and 7d, and 10c and 10d), as C1 leaves the TP and weakens rapidly, the cyclonic shear line also contracts northwestward; A1 moves from the northeastern to the northwestern part of the TP, with enhanced intensity and an expanded range. Positive heat sources turn into negative heat sources over the TPSR (Figs 7c–7d). The anomalous rain bands over the TP gradually weaken to the west, and the east and hinterland of the TP feature negative precipitation anomalies (Figs 10c–10d). The southern edge of the TP is still under the control of the easterly airflow, the negative heat source is maintained (Figs 7c–7d), and precipitation is relatively less (Figs 10c–10d). Associated with the westerly winds on the south side of the wind shear, a weakened northwest–southeast rain belt moves to the Iranian Plateau, to north of the Indian Peninsula, and to the central part of the BOB.

In contrast to Phase 1, in Phase 5, C1 disappears, the centre of A1 reaches the northwest of the TP, and a new anomalous cyclonic circulation (marked as C2) is regenerated in the northeast of the TP. The evolutionary processes of Phases 5–8 are similar to those of Phases 1–4, but have the opposite signs (Figs 9e–9h, 7e–7h and 10e–10h).

In order to demonstrate the westward propagation of the QBWO, the average phase–longitude profiles of the summer intraseasonal geopotential height field along 30°–45°N are given in Fig. 11. At 200 hPa (Fig. 11a) and 500 hPa (Fig. 11b), the QBWO signals propagate from East Asia to West Asia, and the anomalous signals in the middle and upper troposphere are basically consistent, showing a quasi-barotropic structure.

The above analysis indicates that the first two leading modes of the atmospheric intraseasonal heat source over the TPSR present the characteristics of a QBWO propagating from east to west. Associated with the above propagation, large anomalous cyclonic and anticyclonic circulations move in the mid–upper troposphere in an organized way from the northeast of China, over the TP, to reach West Asia. The intensity of the QBWO increases rapidly as it approaches the TP and weakens significantly when leaving the TP.

b *Eastward Propagation Mode of the QBWO of the Atmospheric Heat Source Over the TP*
Similarly, based on the composite phases of PC1 and PC3, the propagation of the QBWO of the diabatic heating source and OLR fields are analyzed, as shown in Fig. 12.

In Phase 1 (Fig. 12a), the TP is dominated by an anomalous heat source, except in the western hinterland, with a strong centre located over the northeastern part of the TP. The anomalous heat source extends to the Northeast Plain. The southern edge of the TP to the northern part of the BOB is also a significant area for atmospheric intraseasonal heat source activity. Negative heat sources prevail over the eastern part of the Iranian Plateau to the northern part of the Indian Peninsula.

Subsequently, in Phases 2–4 (Figs 12b–12d), the anomalous atmospheric heat source moves eastward over the TP. After moving out of the TP, its intensity rapidly weakens and the range narrows. Finally, the signal of the intraseasonal heat source disappears in the region south of the Yangtze River. During this period, a negative heat source anomaly originating from the Iranian Plateau propagates and enters the TP with enhanced intensity, replacing the previous positive heat source anomaly over the TP.

In Phases 5–8, the negative heat source over the TP continues to move eastward, finally reaching the North China Plain, before weakening. The heat source anomaly moves from the eastern part of the Iranian Plateau, toward the TP, and its strength increases. Thus, the anti-phase cycle is retained, with the opposite sign to Phases 1–4.

The sign and strength of the anomalous heat source at the southern edge of the TP to the northern part of the BOB are almost consistent with those of the northeastern part of the TP. With the anomalous heat source in the northeastern part of the TP moving away from the plateau, the heat source at the southern edge of the TP begins to shrink in situ without propagation.
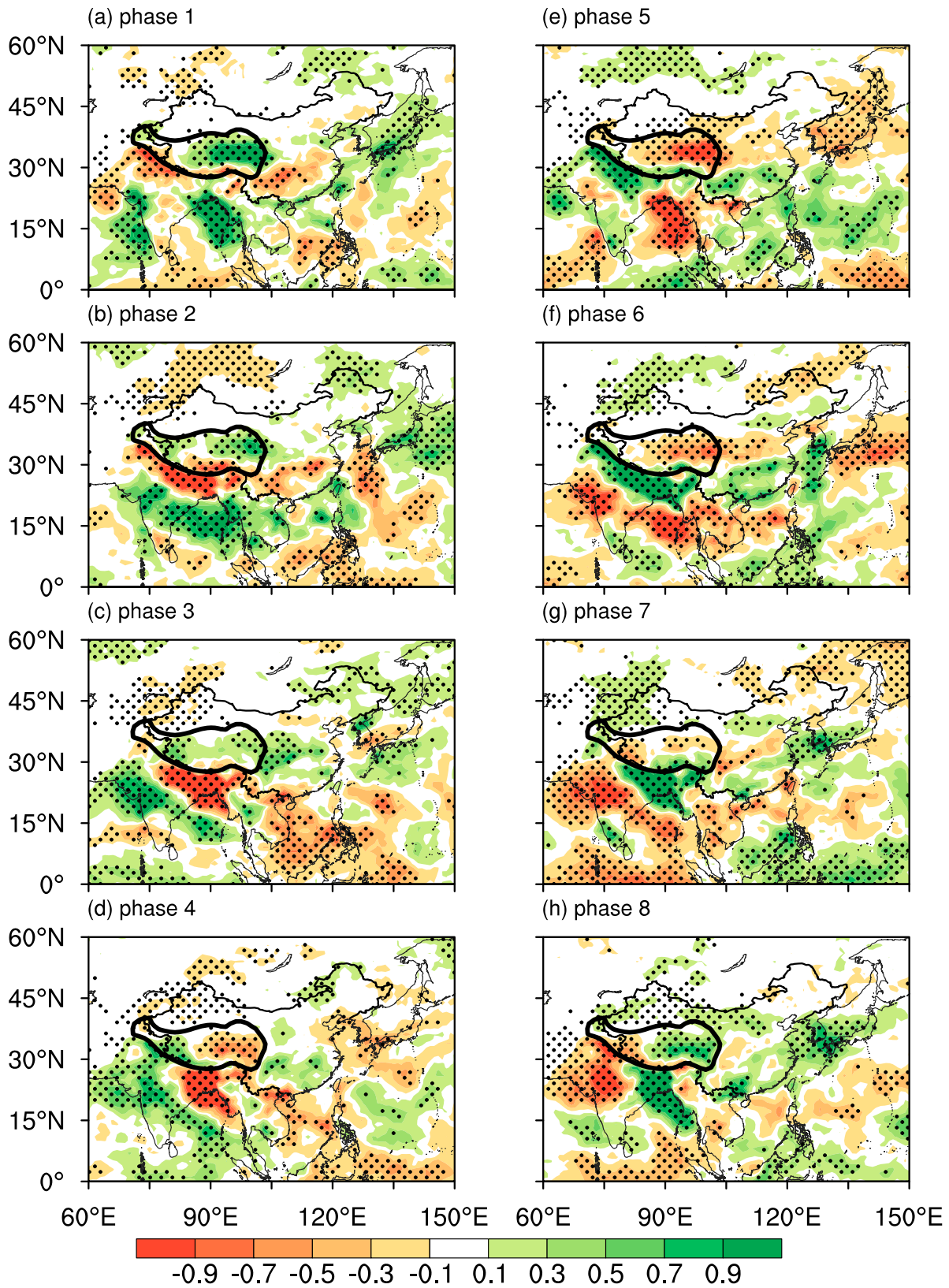
Fig. 10 Evolution of the summer 10–20-day anomalous precipitation field (mm) with phase in the summers of 1979–2018 (based on the composite phases of PC1 and PC2) (the dotted areas are significant at the 0.05 level; the solid black line indicates the 3000 m terrain contour).
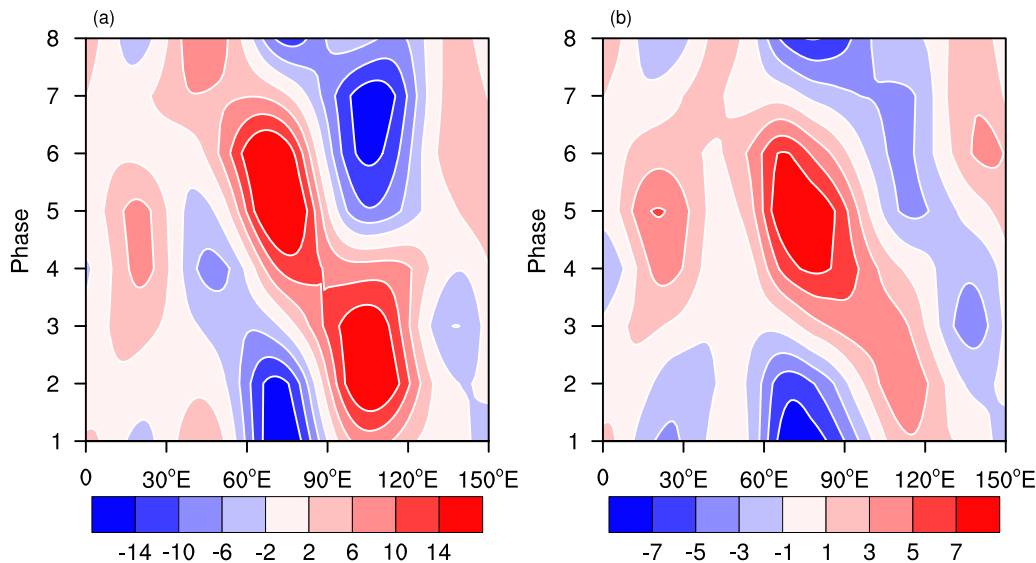
Fig. 11   Average phase–longitude profile of the summer 10–20-day potential height field along 30°–45°N (based on the composite phases of PC1 and PC2): (a) 200 hPa and (b) 500 hPa (gpm).

Corresponding to the anomalous evolution of the above-mentioned atmospheric heat source, the evolutionary phases of the 200 hPa intraseasonal circulation in the upper troposphere are shown in Fig. 13. The centres of intraseasonal circulation anomalies are almost all active between 30°N and 50°N, forming a Rossby wave train from southern Europe, through the TP, to the East Asian coast.

For convenience of description, the anomalous anticyclones (A) and cyclones (C) in Fig. 13 are denoted by the numbers 1 and 2, respectively. In Phase 1 (Fig. 13a), four anomalous circulation centres, marked as C1, A1, C2, and A2, are arranged in order from southern Europe to northeast Asia. To the west of 90°E, the intensities of the anomalous circulations C1, A1, and C2 increase sequentially to the east, and the strongest cyclonic anomaly centre (C2) is located in the northwestern part of the TP. To the east of 90°E, the anomalous anticyclone A2 extends from the eastern part of the TP to the East Asian coast.

In Phase 2, C2 moves eastward from the TP to the Tarim Basin, and its intensity weakens. Over the northeastern part of the TP, A2 remains stable and enhances in situ. In Phases 3–4, the intensity of A1 strengthens significantly as it approaches the TP. After reaching the northwest of the TP, it expands eastward and connects with A2 to form a band of anomalous high pressure. Because of the strong high pressure on both sides of C1, it is pushed northward to the northern Mongolian Plateau, and its intensity falls to a minimum.

In Phases 5–8, A2, which is stable and less mobile in the northeastern part of the TP, merges with the powerful A1 and quickly attenuates and retreats southeastward to south of the Yangtze River; C2 quickly replaces A2 and maintains stability over the eastern TP. Then, the developed C1 merges with C2, forcing A1 to weaken northward. Finally, A1 replaces C2 to start a new cycle with the opposite sign to Phases 1–4.

It can be seen that there are obvious differences in the intensity of the wave train between the east and west sides of the TP. To the west of 90°E, the intensity of the QBWO is enhanced when moving toward the TP and reaches its maximum over the TP. To the east of 90°E, the circulation anomalies are stable and can sustain about half a cycle. The transformation of circulation anomalies is rapid, which is subject to the eastward movement of circulation anomalies on the western sides of the TP.

The circulation anomalies at 500 hPa (Fig. 14) basically correspond to those at 200 hPa and present a quasi-barotropic structure. For 500 hPa, near the surface of the TP, the intensity and range of the circulation anomalies are stronger than those at 200 hPa over the TP. The centre of the circulation anomalies outside the TP lies mainly between 45°N and 60°N, and the position is slightly north. The evolution of the QBWO of circulation anomalies at 500 hPa, the diabatic heating source (Fig. 12), and the precipitation anomalies (Fig. 15) are combined for the following discussion.

In Phase 1 (Figs 14a, 12a, and 15a), the anomalous cyclonic circulation, C2, is most powerful over the TPSR, with its centre over the northwest of the TP. The maximum vortex curvature of C2 is in the eastern part of the TP, inducing the convergence of water vapour and heat. Therefore, the precipitation is obviously stronger and the atmospheric diabatic heating presents as a heat source anomaly over the eastern part of the TP. The western TP to the Iranian plateau is affected by a southern extension of the anomalous anticyclonic circulation of A1 near the Ural Mountains, leading to a negative heat source and less precipitation. On the south side of the TP to the northern part of the BOB, the westerly airflow at the bottom of C2 enhances the summer monsoon, intensifies the convective convergence, and leads to more precipitation and a strengthened heat source.
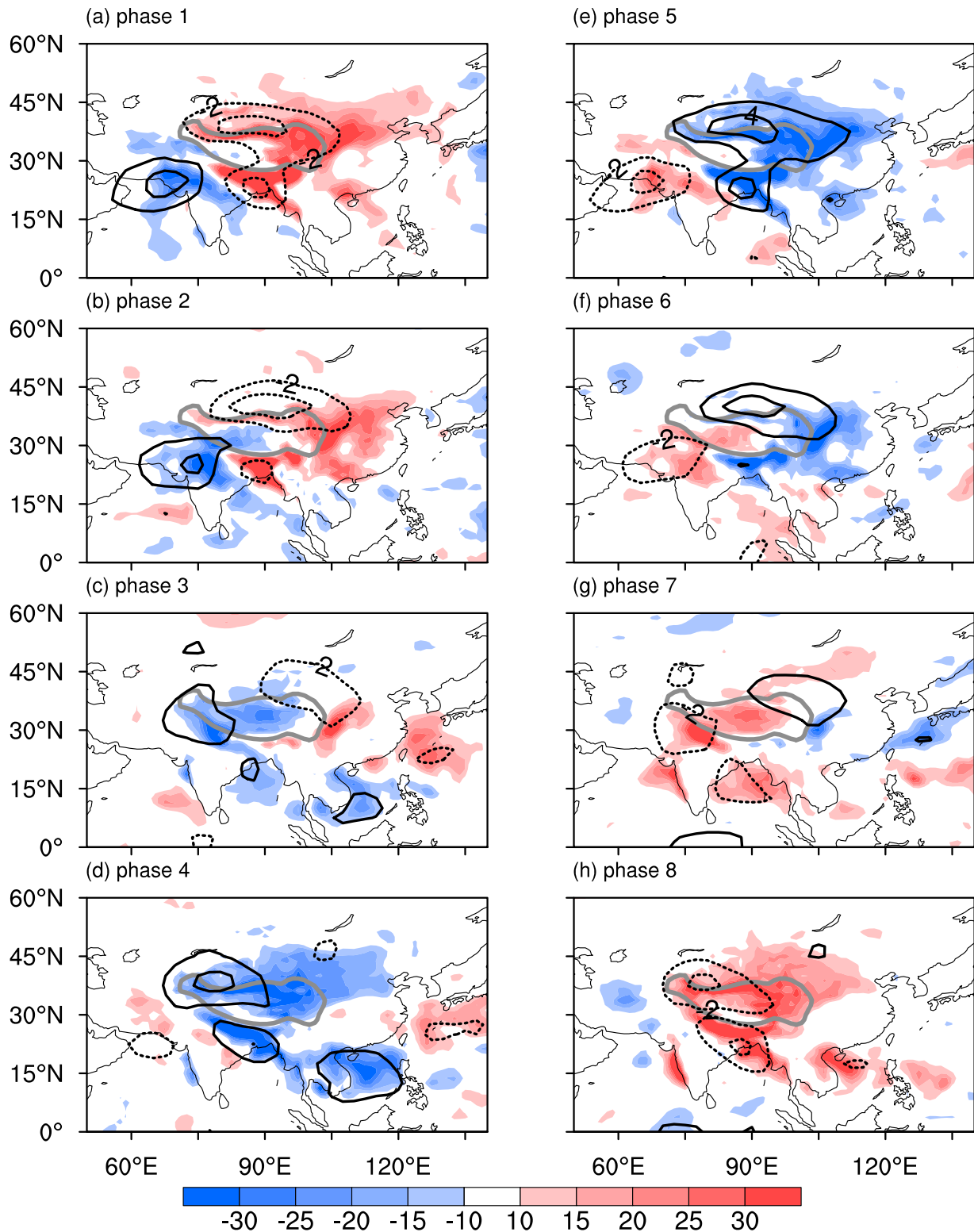
Fig. 12 Evolution of the 10–20-day atmospheric heat source during the summers of 1979–2018 (based on the composite phases of PC1 and PC3) (shading; W m^{-2}) and OLR field (contours; W m^{-2}) (contours and shaded areas are significant at the 0.05 level; solid grey lines indicate the 3000 m terrain contour). The solid and dashed lines represent the positive and negative values, respectively.
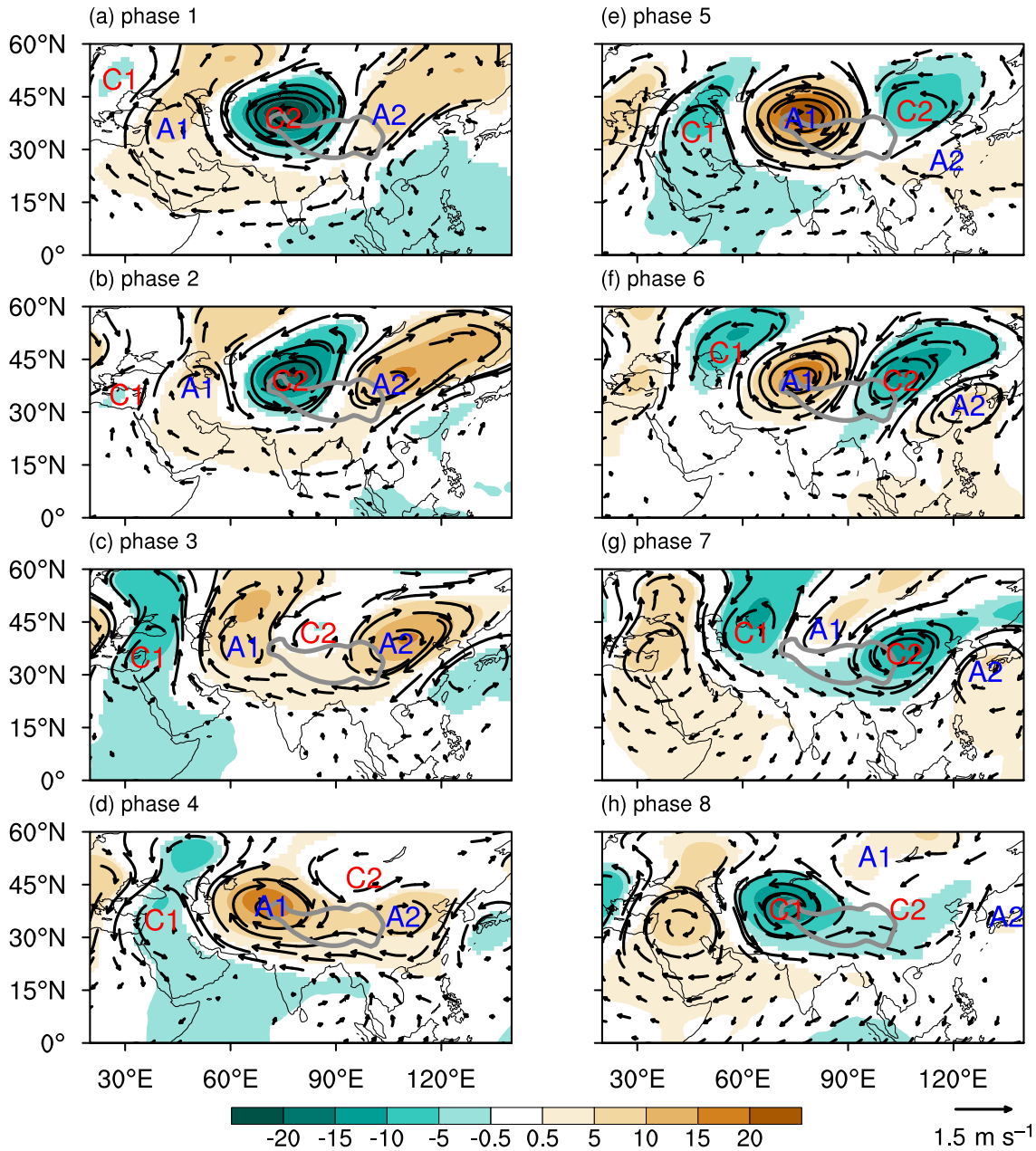
Fig. 13   Evolution of the 200 hPa 10–20-day wind field (vectors; m s^{-1}) and potential height field (shading; gpm) during the summers of 1979–2018 with phase (based on the composite phases of PC1 and PC3) (vectors and shaded areas are significant at the 0.05 level; solid grey lines indicate the 3000 m terrain contour).

In Phase 2 (Figs 14b, 12b, and 15b), C2 moves eastward, with the centre located in the vicinity of the Tarim Basin on the north side of the TP, and is slightly weakened. Correspondingly, the atmospheric heat source and precipitation zone weaken to the east. On the west side of the TP, as A1 extends southward to the Iranian Plateau, the negative heat source enhances and expands eastward, and areas of less precipitation also move to the east.

Figures 14c, 12c, and 15c show that in Phase 3 a circulation pattern is formed with A1 over the western TP and A2 over the eastern TP. Under the high pressure on both sides, C2 is carried northward to the TP near the Altai Mountains and then fills and weakens. Located in the cyclonic shear zone between the two high pressure systems of the northerly and southerly winds, more precipitation occurs over the eastern part of the TP and the southwestern part of China. Meanwhile, less precipitation and a negative heat source appear in the hinterland and the west of the TP because of the strengthening of the anticyclonic anomaly, A1.

In Phase 4 (Figs 12d, 14d, and 15d), A1 increases rapidly over the TP and merges with A2, forming a large and strong anticyclonic circulation. Correspondingly, the
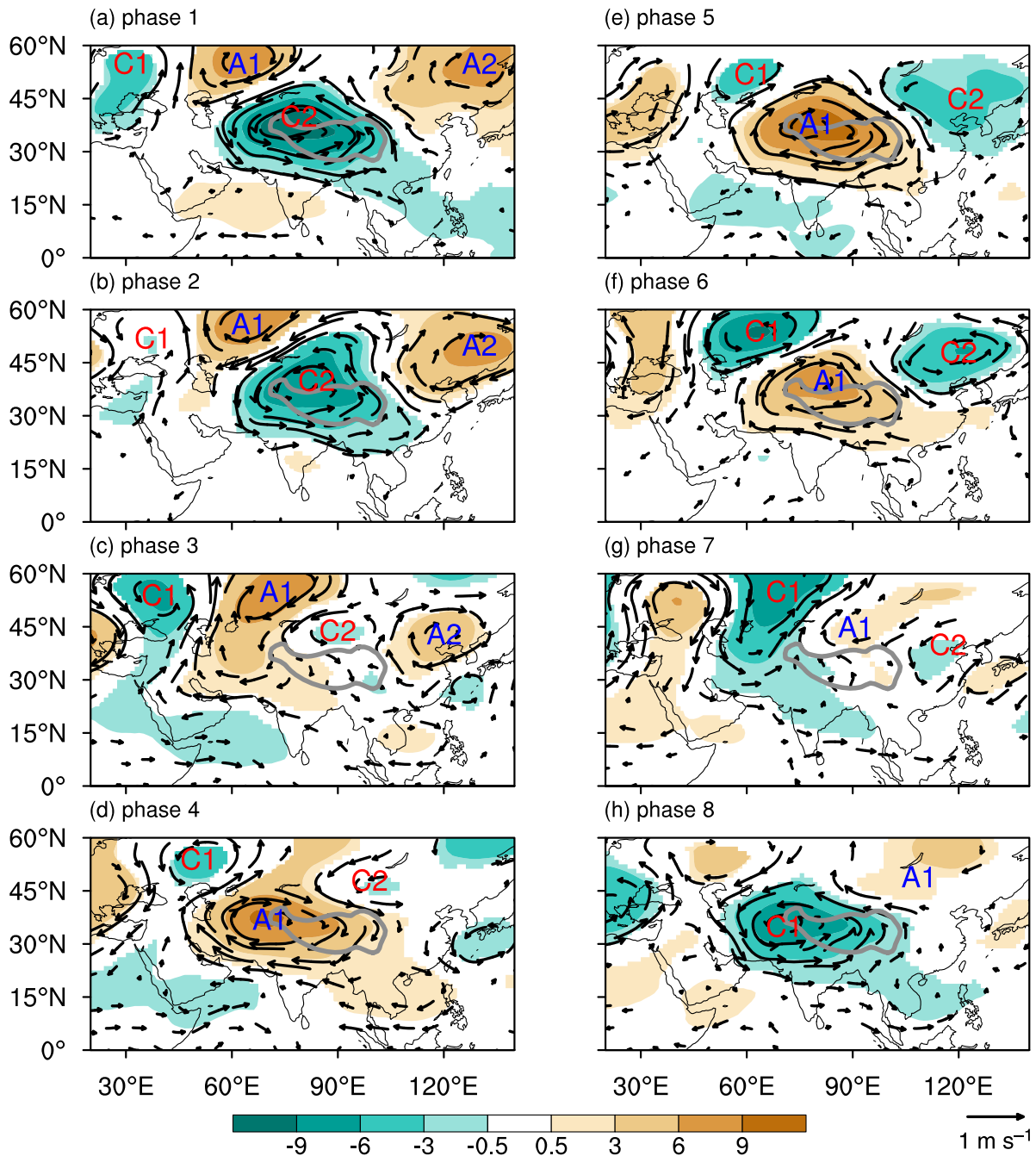
Fig. 14 Evolution of the 500 hPa 10–20-day wind field (vectors; m s^{-1}) and potential height field (shading; gpm) with phase in the summers of 1979–2018 (based on the composite phases of PC1 and PC3) (vectors and shaded areas are significant at the 0.05 level; solid grey lines indicate the 3000 m terrain contour).

intensity and range of the negative heat source also reach their strongest points. The precipitation over the entire TP is reduced.

In Phases 5–8 (Figs 12e–12h, 14e–14h, and 15e–15h), as C1 gradually moves eastward to replace A1, the atmospheric heat source again becomes dominant, and the anomalous precipitation over the western part of the TP begins to increase and move eastward.

The composite phase–longitude profile of the summer geopotential height field averaged along 30°–45°N (Fig. 15)

clearly shows the eastward propagation of the QBWO signal. The anomalous signals at 200 and 500 hPa are basically consistent, showing a quasi-barotropic structure.

Therefore, the west-to-east propagation of the QBWO in the diabatic heating field of the TPSR is mainly a result of the eastward transmission of the mid-latitude Rossby wave train from southern Europe, through the TP, to the East Asian coast. Apparent differences exist in the intensity of the wave train on the east and west sides of the TP. To the west of 90°E, the QBWO is enhanced in the process of moving to the TP,
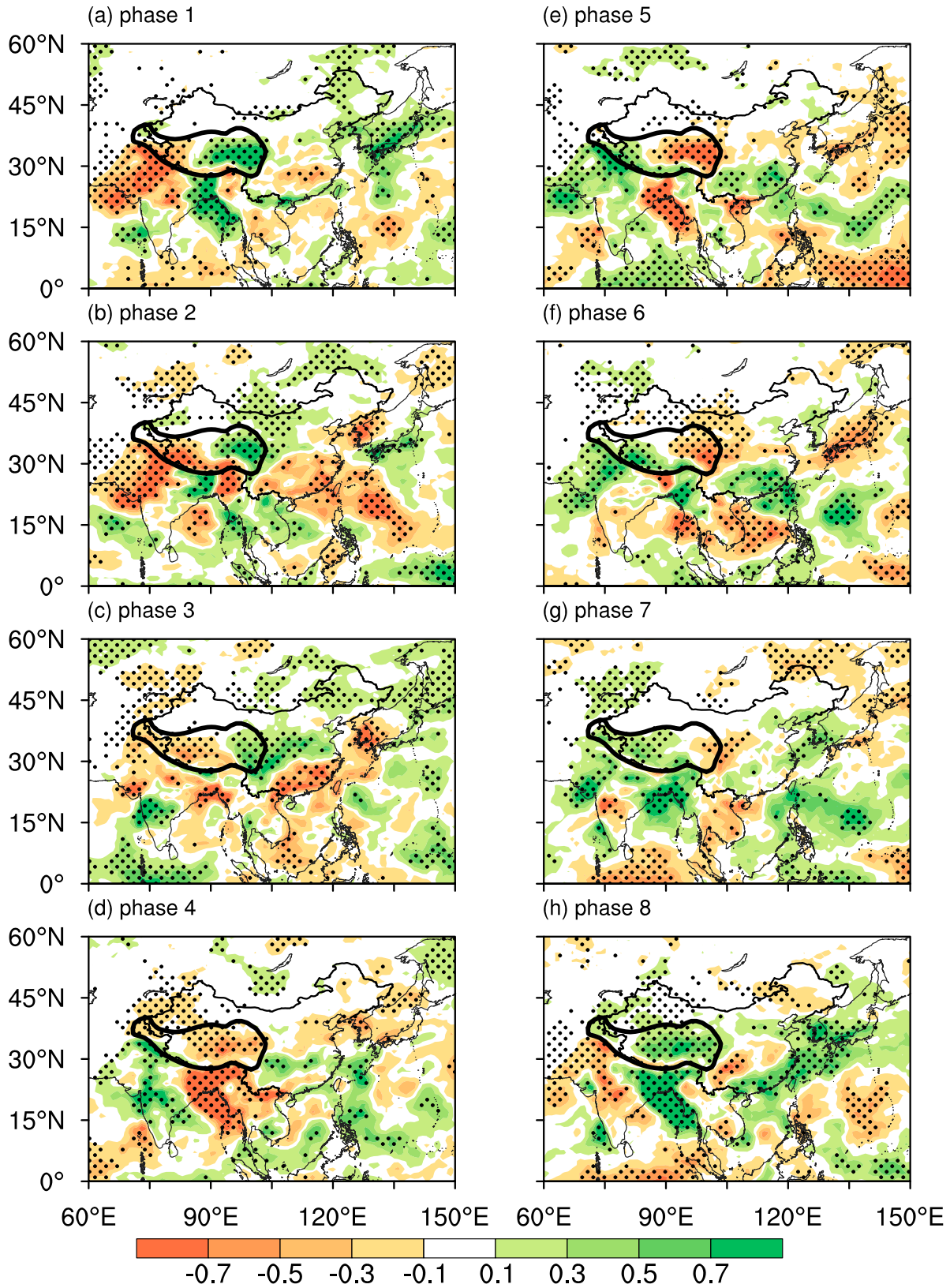
Fig. 15   Evolution of the summer 10–20-day anomalous precipitation field (mm) with phase in the summers of 1979–2018 (based on the composite phases of PC1 and PC3) (dotted areas are significant at the 0.05 level; the solid black line indicates the 3000 m terrain contour).
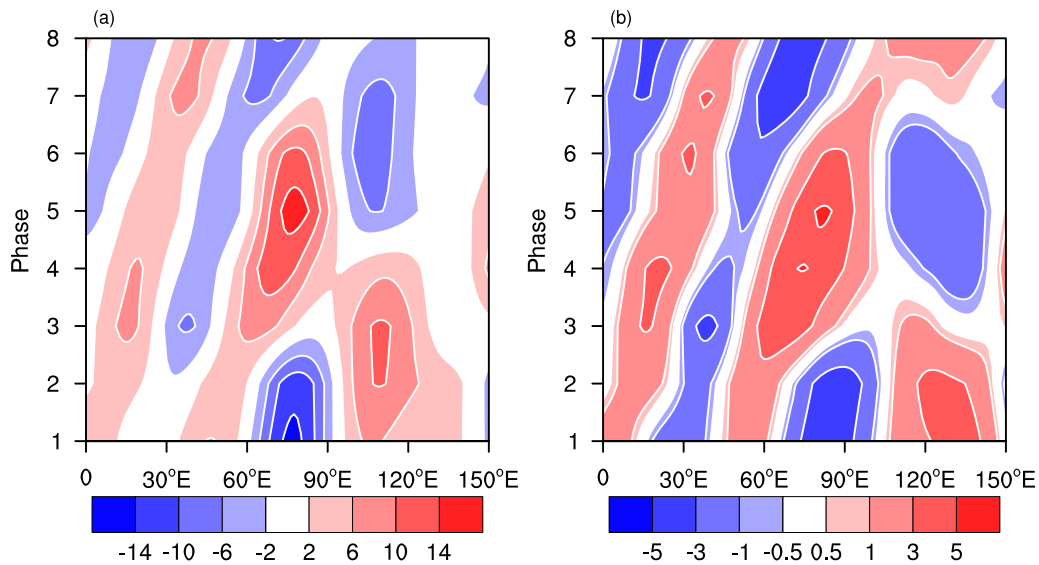
Fig. 16   Average phase–longitude profile of the summer 10–20-day potential height field along 30°–45°N (based on the composite phases of PC1 and PC3): (a) 200 hPa and (b) 500 hPa (gpm).

reaching a maximum over the TP. To the east of 90°E, the anomalous circulation remains stable for half a cycle. Once merged with the enhancing anomalous circulation of the western TP, it quickly weakens to the east and south, and the anomalous signal in the eastern TP quickly switches (Fig. 16).

6 Summary

The TP is an active area of atmospheric ISO in the subtropics and has, therefore, received considerable attention within the research community. However, no consensus has been reached regarding the understanding of the ISO of the TP's thermodynamic effect and its propagation, as well as its mechanism of influence. In our paper, using JRA-55, OLR, and GPCP precipitation data, the main characteristics of the ISO of the apparent atmospheric heat source over the TPSR are investigated, including the dominant periodicity, propagation pathway, and influence on surrounding precipitation. The conclusions can be summarized as follows.

The dominant periodicity of the intraseasonal apparent atmospheric heat source over the TP during the 1979–2018 period is the QBWO of 10–20 days. The first three leading modes of the apparent atmospheric heat source reveal two characteristics of QBWO propagation pathways. The first propagates from east to west. The heat source anomaly moves from the Northeast Plain of China, via the TP, to reach West Asia. On the way, the intensity and range of the heat source are obviously enhanced when approaching the TP and weakened when leaving the TP. This pathway is associated with the middle to upper tropospheric circulation in the mid-latitudes, which is characterized by large-scale anomalous cyclonic and anticyclonic circulations propagating from northeast

China to the west, across the TP, and into West Asia. The intensity of this QBWO increases rapidly when arriving at the TP, and then weakens obviously as it moves away from the TP.

The other pathway propagates from west to east. The heat source anomaly comes from the Iranian Plateau, strengthens over the TP, and, finally, the abnormal signal weakens and disappears in the region south of the Yangtze River. This pathway is closely linked with the mid-latitude Rossby wave train originating from southern Europe that travels through the TP to the East Asian coast. Remarkable differences exist between the intensities of the QBWO wave train over the east and west sides of the TP. To the west of 90°E, the QBWO strengthens as it approaches the TP and reaches its maximum over the TP. To the east of 90°E, the stability of the circulation anomalies is maintained for half a cycle. The phase shift over the eastern TP is very rapid, depending on the intensity of the wave train moving eastward from the western TP.

In addition, the south side of the TP is also an active area of the QBWO of the atmospheric heat source. The intensity of the QBWO changes almost in situ, without clear propagation, in the form of a standing wave.

Through the two propagation pathways, the QBWO of the atmospheric heat source over the TPSR greatly adjusts the circulation and precipitation anomalies over the TP, the Indian Peninsula, and the Indochina Peninsula.

Disclosure statement

No potential conflict of interest was reported by the author(s).

References

Bretherton, C. S., Widmann, M., Dymnikov, V. P., Wallace, J. M., & Blade, I. (1999). The effective number of spatial degrees of freedom of a time varying field. *Journal of Climate*, *12*(7), 1990–2009.

Chen, L. X., & Li, W. L. (1982). The structure of monthly atmosphere heat sources over the Asian monsoon region. In *Proceedings of the National Seminar on Tropical Summer Monsoon (II)* (pp. 246–255). Kunming: Yunnan People's Publishing House (in Chinese).

Duan, A. M., & Wu, G. X. (2005). Role of the Tibetan Plateau thermal forcing in the summer climate patterns over subtropical Asia. *Climate Dynamics*, *24*(7–8), 793–807.

Duan, A. M., Wu, G. X., Liu, Y. M., Ma, Y. M., & Zhao, P. (2012). Weather and climate effects of the Tibetan Plateau. *Advances in Atmospheric Sciences*, *29*(5), 978–992.

Duchon, C. E. (1979). Lanczos filtering in one and two dimensions. *Journal of Applied Meteorology*, *18*(8), 1016–1022.

Flohn, H. (1957). Large-scale aspects of the summer monsoon in South and East Asia. *Journal of the Meteorological Society of Japan*, *75*, 180–186.

Fujinami, H., & Yasunari, T. (2004). Submonthly variability of convection and circulation over and around the Tibetan Plateau during the Boreal Summer. *Journal of the Meteorological Society of Japan*, *82*(6), 1545–1564.

Fujinami, H., & Yasunari, T. (2009). The effects of midlatitude waves over and around the Tibetan Plateau on submonthly variability of the East Asian summer monsoon. *Monthly Weather Review*, *137*(7), 2286–2304.

Hu, W. T., Duan, A. M., Li, Y., & He, B. (2016). The intraseasonal oscillation of Eastern Tibetan Plateau precipitation in response to the summer Eurasian wave train. *Journal of Climate*, *29*, 7215–7230.

Kobayashi, S., Ota, Y., Harada, Y., Ebita, A., Moriya, M., Onoda, H., … Takahashi, K. (2015). The JRA-55 reanalysis: General specification and basic characteristics. *Journal of the Meteorological Society of Japan. Series II*, *93*(1), 5–48.

Li, G. P., Lu, H. G., Huang, C. H., Fan, Y. Y., & Zhang, B. (2016). A climatology of the surface heat source on the Tibetan Plateau in summer and its impacts on the formation of the Tibetan Plateau vortex. *Chinese Journal of Atmospheric Sciences*, *40*(1), 131–141.

Liebmann, B., & Smith, C. A. (1996). Description of a complete (interpolated) outgoing longwave radiation dataset. *Bulletin of the American Meteorological Society*, *77*, 1275–1277.

Lin, H., & Wu, Z. W. (2011). Contribution of the autumn Tibetan Plateau snow cover to seasonal prediction of North American winter temperature. *Journal of Climate*, *24*, 2801–2813.

Lin, H., & Wu, Z. W. (2012). Contribution of Tibetan Plateau snow cover to the extreme winter conditions of 2009/10. *Atmosphere-Ocean*, *50*(1), 86–94.

Liu, H. B., Yang, J., Zhang, D. L., & Wang, B. (2014). Roles of synoptic to quasi-biweekly disturbances in generating the summer 2003 heavy rainfall in East China. *Monthly Weather Review*, *142*(2), 886–904.

Liu, Y. M., Hoskins, B. J., & Blackburn, M. (2007). Impact of Tibetan orography oscillation and heating on the summer flow over Asia. *Journal of the Meteorology Society of Japan*, *85*(B), 1–19.

Ma, L. B., Zhu, Z. W., Li, J., & Cao, J. (2019). Improving the simulation of the climatology of the East Asian summer monsoon by coupling the Stochastic Multicloud Model to the ECHAM6.3 atmosphere model. *Climate Dynamics*, *53*(3–4), 2061–2081.

Matthews, A. J. (2000). Propagation mechanisms for the Madden-Julian Oscillation. *Quarterly Journal of the Royal Meteorological Society*, *126*(569), 2637–2651.

North, G. R., Bell, T. L., Cahalan, R. F., & Moeng, F. J. (1982). Sampling errors in the estimation of empirical orthogonal functions. *Monthly Weather Review*, *110*(7), 699–706.

Tao, S. Y., & Ding, Y. H. (1981). Observation evidence of the influence of the Tibet Plateau on the occurrence of heavy rain and severe convective storms in China. *Bulletin of the American Meteorological Society*, *62*(1), 23–30.

Wang, L. J., Dai, A. G., Guo, S. H., & Ge, J. (2017). Establishment of the South Asian high over the Indo-China Peninsula during late spring to summer. *Advances in Atmospheric Sciences*, *34*, 169–180.

Wang, M. R., & Duan, A. M. (2015). Quasi-biweekly oscillation over the Tibetan Plateau and its link with the Asian Summer Monsoon. *Journal of Climate*, *28*(12), 4921–4940.

Wang, M. R., Wang, J., Duan, A. M., Liu, Y. M., & Zhou, S. W. (2018). Coupling of the quasi-biweekly oscillation of the Tibetan Plateau summer monsoon with the Arctic oscillation. *Geophysical Research Letters*, *45*, 7756–7764.

Watanabe, T., & Yamazaki, K. (2012). Influence of the anticyclonic anomaly in the subtropical jet over the western Tibetan Plateau on the intraseasonal variability of the summer Asian monsoon in early summer. *Journal of Climate*, *25*(4), 1291–1303.

Wu, G. X., Liu, Y. M., He, B., Bao, Q., Duan, A. M., & Jin, F. F. (2012). Thermal controls on the Asian summer monsoon. *Scientific Reports*, *2*, 404. doi:10.1038/srep00404

Wu, G. X., Liu, Y. M., Wang, T. M., Wan, R., Liu, X., Li, W. P., … Liang, X. Y. (2006). The influence of mechanical and thermal forcing by the Tibetan Plateau on Asian climate. *Journal of Hydrometeorology*, *8*(4), 770–789.

Wu, G. X., & Zhang, Y. S. (1998). Tibetan Plateau forcing and the timing of the monsoon onset over South Asia and the South China Sea. *Monthly Weather Review*, *126*(4), 913–927.

Wu, Z. W., Jiang, Z., Li, J., Zhong, S., & Wang, L. (2012). Possible association of the western Tibetan Plateau snow cover with the decadal to interdecadal variations of northern China heatwave frequency. *Climate Dynamics*, *39*, 2393–2402.

Wu, Z. W., Li, J., Jiang, Z., & Ma, T. (2012). Modulation of the Tibetan Plateau snow cover on the ENSO teleconnections: From the East Asian summer monsoon perspective. *Journal of Climate*, *25*, 2481–2489.

Wu, Z. W., Zhang, P., Chen, H., & Li, Y. (2016). Can the Tibetan Plateau snow cover influence the interannual variations of Eurasian heat wave frequency? *Climate Dynamics*, *46*, 3405–3417.

Xu, X. D., Zhao, T. L., Shi, X. H., & Lu, C. G. (2015). A study of the Tibetan Plateau's thermal forcing in modulating rainband and moisture transport in eastern China. *Acta Meteorologica Sinica*, *73*(1), 20–35.

Yanai, M., Li, C. F., & Song, Z. S. (1992). Seasonal heating of the Tibetan Plateau and its effects on the evolution of the Asian summer monsoon. *Journal of the Meteorological Society of Japan*, *70*(1), 319–351.

Yang, H., & Li, C. Y. (2003). The relation between atmospheric intraseasonal oscillation and summer severe flood and drought in the Changjiang–Huaihe River basin. *Advances in Atmospheric Sciences*, *20*, 540–553.

Yang, J., Bao, Q., Wang, B., Gong, D. Y., He, H., & Gao, M. N. (2014). Distinct quasi-biweekly features of the subtropical East Asian monsoon during early and late summers. *Climate Dynamics*, *42*(5–6), 1469–1486.

Yang, J., Bao, Q., Wang, B., He, H. Z., Gao, M. N., & Gong, D. Y. (2017). Characterizing two types of transient intraseasonal oscillations in the

eastern Tibetan Plateau summer rainfall. *Climate Dynamics*, *48*(5–6), 1749–1768.

Yang, S. Y., & Li, T. (2017). The role of intraseasonal variability at mid-high latitudes in regulating Pacific blockings during boreal winter. *International Journal of Climatology*, *37*, 1248–1256.

Yasunari, T., & Miwa, T. (2006). Convective cloud systems over the Tibetan Plateau and their impact on meso-scale disturbances in the Meiyu/Baiu frontal zone—A case study in 1998. *Journal of the Meteorological Society of Japan*, *84*, 783–803.

Ye, D. Z., Luo, S. W., & Zhu, B. Z. (1957). Structure of the circulation fields over Tibetan Plateau and surrounding areas and thermal balance of the tropospheric atmosphere. *Acta Meteorologica Sinica*, *28*(2), 108–121.

Ye, D. Z., & Wu, G. X. (1998). The role of the heat source of the Tibetan Plateau in the general circulation. *Meteorology and Atmospheric Physics*, *67*(1–4), 181–198.

Zhang, P. F., Li, G. P., Fu, X. H., Liu, Y. M., & Li, L. F. (2014). Clustering of Tibetan Plateau vortices by 10-30-day intraseasonal oscillation. *Monthly Weather Review*, *142*(1), 290–300.

Zhong, S. S., He, J. H., Guan, Z. Y., & Wen, M. (2009). Climatic characteristics of the atmospheric heat source over the Tibetan Plateau during 1961–2001. *Acta Meteorologica Sinica*, *67*(3), 407–416. (in Chinese).

Zhong, S. S., Wu, Z. W., & He, J. H. (2013). Comparisons of the thermal effects of the Tibetan Plateau with NCEP-I and ERA-40 reanalysis data. *Atmosphere-Ocean*, *51*(1), 75–87.